J|A|C|S
ARTICLES
Published on Web 01/11/2006

Mono-, Di-, Tri-, and Tetra-Substituted Fluorotyrosines: New Probes for Enzymes That Use Tyrosyl Radicals in Catalysis†

Mohammad R. Seyedsayamdost, Steven Y. Reece, Daniel G. Nocera,* and JoAnne Stubbe*

Contribution from the Department of Chemistry, Massachusetts Institute of Technology, 77 Massachusetts Avenue, Cambridge, Massachusetts 02139-4307

Received August 28, 2005; E-mail: nocera@mit.edu; stubbe@mit.edu

Abstract: A set of *N*-acylated, carboxyamide fluorotyrosine (F_nY) analogues [Ac−3-FY−NH_2, Ac−3,5-F_2Y−NH_2, Ac−2,3-F_2Y−NH_2, Ac−2,3,5-F_3Y−NH_2, Ac−2,3,6-F_3Y−NH_2 and Ac−2,3,5,6-F_4Y−NH_2] have been synthesized from their corresponding amino acids to interrogate the detailed reaction mechanism(s) accessible to F_nY•s in small molecules and in proteins. These Ac−F_nY−NH_2 derivatives span a pK_a range from 5.6 to 8.4 and a reduction potential range of 320 mV in the pH region accessible to most proteins (6−9). DFT electronic-structure calculations capture the observed trends for both the reduction potentials and pK_as. Dipeptides of the methyl ester of 4-benzoyl-L-phenylalanyl-F_nYs at pH 4 were examined with a nanosecond laser pulse and transient absorption spectroscopy to provide absorption spectra of F_nY•s. The EPR spectrum of each F_nY• has also been determined by UV photolysis of solutions at pH 11 and 77 K. The ability to vary systematically both pK_a and radical reduction potential, together with the facility to monitor radical formation with distinct absorption and EPR features, establishes that F_nYs will be useful in the study of biological charge-transport mechanisms involving tyrosine. To demonstrate the efficacy of the fluorotyrosine method in unraveling charge transport in complex biological systems, we report the global substitution of tyrosine by 3-fluorotyrosine (3-FY) in the R2 subunit of ribonucleotide reductase (RNR) and present the EPR spectrum along with its simulation of 3-FY122•. In the companion paper, we demonstrate the utility of F_nYs in providing insight into the mechanism of tyrosine oxidation in biological systems by incorporating them site-specifically at position 356 in the R2 subunit of *Escherichia coli* RNR.

Introduction

Electron transfer (ET) has been the focus of most studies of charge transport in biology. Proteins modified with redox-active donors and acceptors,[1−5] protein partners,[6−10] and DNA bioconjugates[11−14] reveal that electrons transfer over long distances according to the Marcus theory of ET,[15] augmented by considerations for electron tunneling.[16,17] In functioning enzymes, however, the occurrence of isolated ET is uncommon. Many primary metabolic steps involving charge transport rely on amino acid radicals in which ET is coupled to proton transfer (PT).[18−21] For such charge-transport reactions, the problem is intrinsically more complicated because both the electron and proton tunnel and these tunneling events can be coupled to one another.[22,23] As the electron moves, the pK_a of the oxidized cofactor will change; however, to predict kinetics, knowledge of the driving forces for the ET and PT reactions is insufficient. The reorganization energy will be affected by the charge redistribution resulting from electron and proton motion.[24−27] In addition, the electronic coupling will change parametrically with the proton coordinate.

Of the amino acid radicals participating in biological charge-transfer processes, tyrosyl radical (Y•) is pre-eminent.[20,21,28] This

† Authors' note: F_nY refers to unprotected fluorotyrosines with free N- and C- termini while Ac−F_nY−NH_2 refers to *N*-acylated, carboxyamide-protected fluorotyrosines.

(1) *Electron Transfer in Chemistry*; Balzani, V., Ed.; Wiley-VCH: Weinheim, Germany, 2001; Vol. 3, Part 1.
(2) Gray, H. B.; Winkler, J. R. *Annu. Rev. Biochem.* **1996**, *65*, 537.
(3) Gunner, M. R.; Robertson, D. E.; Dutton, P. L. *J. Phys. Chem.* **1986**, *90*, 3783.
(4) Farver, O.; Pecht, I. *Biophys. Chem.* **1994**, *50*, 203.
(5) Namslauer, A.; Braenden, M.; Brzezinski, P. *Biochemistry* **2002**, *41*, 10369.
(6) Tollin, G. In *Electron Transfer in Chemistry*; Balzani, V., Ed.; Wiley-VCH: Weinheim, Germany, 2001; Vol. 4, Part 1, p 202.
(7) Davidson, V. L. *Acc. Chem. Res.* **2000**, *33*, 87.
(8) McLendon, G.; Hake, R. *Chem. Rev.* **1992**, *92*, 481.
(9) Millett, F.; Durham, B. *Biochemistry* **2002**, *41*, 11315.
(10) Nocek, J. M.; Zhou, J. S.; Forest, S. D.; Priyadarshy, S.; Beratan, D. N.; Onuchic, J. N.; Hoffman, B. M. *Chem. Rev.* **1996**, *96*, 2459.
(11) Lewis, F. D. Electron Transfer and Charge Transport in DNA. In *Electron Transfer in Chemistry*; Balzani, V., Ed.; Wiley-VCH: Weinheim, Germany, 2001; Vol. 3, Part 5, p 105.
(12) Boon, E. M.; Barton, J. K. *Curr. Opin. Struct. Biol.* **2002**, *12*, 320.
(13) Giese, Bernd. *Curr. Opin. Chem. Biol.* **2002**, *6*, 612.
(14) Jortner, J.; Bixon, M.; Langenbacher, T.; Michel-Beyerle, M. E. *Proc. Natl. Acad. Sci. U.S.A.* **1998**, *95*, 12759.
(15) Marcus, R. A.; Sutin, N. *Biochim. Biophys. Acta* **1985**, *811*, 265.
(16) Hopfield, J. J. *Proc. Natl. Acad. Sci. U.S.A.* **1974**, *71*, 3640.
(17) Levich, V. G. *Adv. Electrochem. Electrochem. Eng.* **1966**, *4*, 249.
(18) Stubbe, J.; Nocera, D. G.; Yee, C. S.; Chang, M. C. Y. *Chem. Rev.* **2003**, *103*, 2167.
(19) Chang, C. J.; Chang, M. C. Y.; Damrauer, N. H.; Nocera, D. G. *Biochim. Biophys. Acta* **2004**, *1655*, 13.
(20) Stubbe, J.; van der Donk, W. A. *Chem. Rev.* **1998**, *98*, 705.
(21) Stubbe, J. *Chem. Comm.* **2003**, *20*, 2511.
(22) Cukier, R. I.; Nocera, D. G. *Annu. Rev. Phys. Chem.* **1998**, *49*, 337.
(23) Hammes-Schiffer, S. *Acc. Chem. Res.* **2001**, *34*, 273.
(24) Cukier, R. I. *J. Phys. Chem.* **1995**, *99*, 16101.
(25) Cukier, R. I. *J. Phys. Chem. A* **1999**, *103*, 5989.
(26) Soudackov, A. V.; Hammes-Schiffer, S. *J. Chem. Phys.* **1999**, *111*, 4672.
(27) Soudackov, A.; Hammes-Schiffer, S. *J. Chem. Phys.* **2000**, *113*, 2385.
(28) Pesavento, R. P.; van der Donk, W. A. *Adv. Protein Chem.* **2001**, *58*, 317.

one-electron, protein-based oxidant has been identified as both a stable cofactor in deoxynucleotide biosynthesis[29] and as a transient intermediate with directed reactivity in photosynthetic O_2 evolution,[30] prostaglandin biosynthesis,[31] and disproportionation of hydrogen peroxide.[32] Despite extensive knowledge about the structure of the Y•s in these systems and the ever increasing number of Y•s identified in other proteins,[33−35] the precise mechanism of their formation and reactivity at a functional biological level has, for the most part, remained unknown. However, at a mechanistic level, it is well established that oxidation of tyrosine under physiological conditions requires the loss of both a proton and an electron, implicating proton-coupled electron transfer (PCET) in the radical-forming mechanism.[18,30,36] Therefore, the study of Y•s in the initiation and propagation of charge in biology will necessarily demand that new tools are needed to control both the electron and proton for Y• formation within the enzyme. This is especially pertinent to our studies of class I ribonucleotide reductase (RNR), where reversible radical transfer is proposed to occur between a stable Y122 radical (Y122•) on the R2 subunit and C439 on the R1 subunit.[18,37] Radical migration over this unprecedented distance has been suggested to involve a radical-hopping pathway spanning both subunits with three other tyrosine residues, Y356 (R2), 731 (R1), and 730 (R1), leading into the R1 active site. Moreover, the mechanism of formation of the stable Y122•, which involves a putative di-iron, Fe^{III}/Fe^{IV} intermediate as the oxidant, also remains unknown.[38−42]

Substitution of tyrosine with other redox-active amino acids can provide insight into the mechanism of charge transport in enzymes. However, only the natural amino acids tryptophan and cysteine have reduction potentials close to that of tyrosine, and they are poor structural substitutes. For this reason, we have turned our attention to unnatural amino acids, specifically fluorotyrosines, because they offer minimal structural perturbations compared to tyrosine. They are isosteric with tyrosine, and the van der Waals radius of fluorine is only 0.15 Å larger than that of hydrogen, thus representing the most conservative substitution barring isotopic replacement. Fluorination at various points on the phenol ring affects a large range of pK_a values for the unprotected amino acid (F_nYs).[43] A similar variation in the tyrosyl radical-reduction potentials upon fluorine substitution would provide a systematic variation in ΔG°_{ET} and ΔG°_{PT}, the factors that control the thermodynamics of PCET reactions.

Chart 1

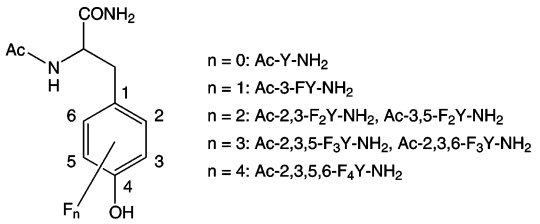

In this paper we report the synthesis and physical characterization of the *N*-acetyl and *C*-amide protected fluorotyrosines, Ac−F_nY−NH_2s, shown in Chart 1. We also develop the methodologies for determining the ΔG°_{ET} and ΔG°_{PT} for the half of the PCET reaction involving fluorotyrosine oxidation by measuring the reduction potentials for the radicals and the pK_a of the phenolic protons for Ac−F_nY−NH_2s, the latter of which is shown to vary by up to 0.4 pK_a units when compared to F_nYs. Furthermore, we report the spectroscopic properties of the F_nY•s, both EPR spectra and UV/vis absorbance spectra, using transient laser-absorption spectroscopy. To demonstrate the efficacy of the fluorotyrosine method in unraveling charge transport in biological systems of complexity, we report the global substitution of tyrosine by 3-fluorotyrosine (3-FY) in R2 and present the EPR spectrum of the 3-FY122•, along with its simulation. In the companion paper,[44] we demonstrate the utility of F_nYs in providing insight into the mechanism of tyrosine oxidation in biological systems by incorporating them site-specifically at position 356 in the R2 subunit of *Escherichia coli* RNR and correlating RNR activity to reduction potentials of the Ac−F_nY−NH_2s presented here.

Experimental Section

Materials and Methods. All fluorinated phenols, sodium pyruvate, pyridoxal-5′-phosphate (PLP), *N*-acetyl-L-tryosinamide, 3-fluoro-L-tyrosine, trifluoroacetic acid (TFA), thionyl chloride, acetic anhydride, triethylamine, gaseous ammonia, 1-(3-(dimethylamino)-propyl)-3-ethylcarbodiimide hydrochloride, and *N*-methylmorpholine (NMM) were purchased from Sigma-Aldrich. L-Tyrosine methyl ester hydrochloride (Y−OMe•HCl) and 4-benzoyl-*N*-[(1,1-dimethylethoxy) carbonyl]-L-phenylalanine (Boc−BPA−OH) were from Advanced ChemTech. 1-Hydroxybenzotriazole (HOBt) was obtained from NovaBiochem. All chemicals were used as received.

Synthesis of F_nYs. The plasmid, pTZTPL, encoding the enzyme tyrosine phenol lyase (TPL), was a generous gift of Prof. Robert Phillips. TPL purifications were carried out as described.[45] F_nYs were synthesized by stirring a 1 L solution of 30 mM ammonium acetate, pH 8.0, 10 mM of the appropriate fluorophenol, 60 mM sodium pyruvate, 5 mM β-mercaptoethanol, 40 μM PLP, and 30 units of TPL at room temperature for 3−4 days in the dark. Synthesis of 2,3,5,6-tetrafluorotyrosine required 300 units of TPL and a 3−4 week incubation period, with an additional 20 units TPL and 1 mM tetrafluorophenol added every week. It was important to keep the phenol concentration at 10 mM or lower, as higher concentrations resulted in enzyme denaturation. After the incubation period, the mixture was acidified to pH = 3.0 with concentrated HCl. The precipitated protein was removed by filtering the mixture through a 2−3 cm thick Celite pad. The filtrate was extracted once with 0.5 volumes of ethyl acetate. The aqueous layer was loaded onto a 200 mL (4 cm × 17 cm) AG50W−X8 (50−100 mesh) cation-exchange resin in the protonated state. After loading,

(29) Jordan, A.; Reichard, P. *Annu. Rev. Biochem.* **1998**, *67*, 71.
(30) Tommos, C.; Babcock, G. T. *Biochim. Biophys. Acta* **2000**, *1458*, 199.
(31) Karthein, R.; Nastainczyk, W.; Ruf, H. H. *Eur. J. Biochem.* **1987**, *166*, 173.
(32) Chouchane, S.; Girotto, S.; Yu, S.; Magliozzo, R. S. *J. Biol. Chem.* **2002**, *277*, 42633.
(33) Su, C.; Sahlin, M.; Oliw, E. H. *J. Biol. Chem.* **1998**, *273*, 20744.
(34) Ivancich, A.; Dorlet, P.; Goodin, D. B.; Un, S. *J. Am. Chem. Soc.* **2001**, *123*, 5050.
(35) Aubert, C.; Mathis, P.; Eker, A. P. M.; Brettel, K. *Proc. Natl. Acad. Sci. U.S.A.* **1999**, *96*, 5423.
(36) Sjödin, M.; Styring, S.; Wolpher, H.; Xu, Y.; Sun, L.; Hammarström, L. *J. Am. Chem. Soc.* **2005**, *127*, 3855.
(37) Stubbe, J.; Riggs-Gelasco, P. *Trends Biochem. Sci.* **1998**, *23*, 438.
(38) Bollinger, J. M., Jr.; Edmonson, D. E.; Huynh, B. H.; Filley, J.; Norton, J. R.; Stubbe, J. *Science* **1991**, *253*, 292.
(39) Bollinger, J. M., Jr.; Tong, W. H.; Ravi, N.; Huynh, B. H.; Edmonson, D. E.; Stubbe, J. *J. Am. Chem. Soc.* **1994**, *116*, 8015.
(40) Bollinger, J. M., Jr.; Tong, W. H.; Ravi, N.; Huynh, B. H.; Edmondson, D. E.; Stubbe, J. *J. Am. Chem. Soc.* **1994**, *116*, 8024.
(41) Baldwin, J.; Krebs, C.; Ley, B. A.; Edmondson, D. E.; Huynh, B. H.; Bollinger, J. M., Jr. *J. Am. Chem. Soc.* **2000** *122*, 12195.
(42) Krebs, C.; Chen, S.; Baldwin, J.; Ley, B. A.; Patel, U.; Edmondson, D. E.; Huynh, B. H.; Bollinger, J. M., Jr. *J. Am Chem. Soc.* **2000** *122*, 12207.
(43) Kim, K.; Cole, P. A. *J. Am. Chem. Soc.* **1998**, *120*, 6851.
(44) Seyedsayamdost, M. R.; Yee, C. S.; Reece, S. Y.; Nocera D. G.; Stubbe, J. *J. Am. Chem. Soc.* See accompanying paper.
(45) Chen, H.; Gollnick, P.; Phillips, R. S. *Eur. J. Biochem.* **1995**, *229*, 540.

the column was washed with 10 volumes of water. The F_nY analogue was then eluted with a 10% ammonium hydroxide solution. Fractions that gave positive ninhydrin tests (purple stain after heating) were pooled, concentrated in vacuo, lyophilized to dryness, and stored at 4 °C. Yields ranged from 50 to 80% on the basis of the phenol as the limiting reagent. The ninhydrin solution consisted of 0.19% w/v ninhydrin, 95% v/v η-butanol, 0.5% v/v acetic acid, and 4.5% v/v water.

3,5-F_2Y: ^{1}H NMR (300 MHz, D_2O) δ = 3.0 (dd, 1H, $C_\beta-H_1$, 8.2 Hz, 14.7 Hz), 3.18 (dd, 1H, $C_\beta-H_2$, 5.1 Hz, 14.6 Hz), 3.93 (dd, 1H, $C_\alpha-H$, 5 Hz, 8 Hz), 6.88 (m, 2H, aromatic C−H). ^{19}F NMR (300 MHz, D_2O) δ = 26.9 (d, 2F, 8.3 Hz).

2,3-F_2Y: ^{1}H NMR (300 MHz, D_2O) δ = 2.74 (dd, 1H, $C_\beta-H_1$, 7.7 Hz, 13.8 Hz), 2.92 (dd, 1H, $C_\beta-H_2$, 5.8 Hz, 13.8 Hz), 3.43 (dd, 1H, $C_\alpha-H$, 5.8 Hz, 7.7 Hz), 6.46 (m, 1H, aromatic C−H), 6.71 (m, 1H, aromatic C−H). ^{19}F NMR (300 MHz, D_2O) δ = −3.50 (dd, 1F, 8.3 Hz, 19 Hz), 16.8 (dd, 1F, 8.3 Hz, 19.8 Hz).

2,3,5-F_3Y: ^{1}H NMR (300 MHz, D_2O) δ = 2.73 (dd, 1H, $C_\beta-H_1$, 7.5 Hz, 13.9 Hz), 2.89 (dd, 1H, $C_\beta-H_2$, 5.9 Hz, 13.9 Hz), 3.43 (dd, 1H, $C_\alpha-H$, 5.8 Hz, 7.4 Hz), 6.66 (m, 1H, aromatic C−H). ^{19}F NMR (300 MHz, D_2O) δ = 0.28 (dd, 1F, 16.6 Hz, 19.4 Hz), 12.55 (m, 1F) 19.7 (m, 1F).

2,3,6-F_3Y: ^{1}H NMR (300 MHz, D_2O) δ = 3.08 (dd, 1H, $C_\beta-H_1$, 8.2 Hz, 15 Hz), 3.24 (dd, 1H, $C_\beta-H_2$, 5.7 Hz, 9.2 Hz), 3.9 (dd, 1H, $C_\alpha-H$, 5.7 Hz, 8.1 Hz), 6.42 (m, 1H, aromatic C−H). ^{19}F NMR (300 MHz, D_2O) δ = −7 (m, 1F), 19.07 (d, 1F, 22.2 Hz), 38.13 (t, 1F, 11.1 Hz).

2,3,5,6-F_4Y: ^{1}H NMR (300 MHz, D_2O) δ = 3.12 (dd, 1H, $C_\beta-H_1$, 8.3 Hz, 14.9 Hz), 3.27 (dd, 1H, $C_\beta-H_2$, 5.4 Hz, 14.9 Hz), 3.9 (dd, 1H, $C_\alpha-H$, 5.5 Hz, 8 Hz). ^{19}F NMR (300 MHz, D_2O) δ = −5.14 (dd, 2F, 11.1 Hz, 27.8 Hz), 11.81 (dd, 2F, 11.1 Hz, 27.7 Hz).

Synthesis of F_n-Tyrosine Methyl Ester Hydrochloride ($F_nY-OMe\cdot HCl$). In a typical synthesis, the diammonium salt of the F_nY (0.6 mmol) was combined with 20 mL of methanol in a 50-mL round-bottom flask. Thionyl chloride (400 μL, 5.5 mmol) was added dropwise, and the solution was stirred for 3 days at room temperature. The solvent was removed in vacuo, and the resulting white solid was dissolved in a minimal amount of methanol. Ether was added dropwise to precipitate NH_4Cl, which was removed by filtration. Further dropwise addition of ether induced crystallization of the desired compound. After cooling to −20 °C, the white crystals were isolated by filtration and dried in vacuo, providing product in 70−88% yield.

3-FY−OMe·HCl: ^{1}H NMR (300 MHz, $(CD_3)_2SO$, 25 °C) δ = 3.02 (m, 2H, $C_\beta-H$), 3.68 (s, 3H, $-OCH_3$), 4.22 (m, 1H, $C_\alpha-H$), 6.80 (m, 1H, aromatic C−H), 6.90 (m, 1H, aromatic C−H), 7.02 (m, 1H, aromatic C−H), 8.56 (b.s., 3H, $-NH_3^+$), 9.88 (b.s., 1H, PhO−H). ^{19}F NMR (300 MHz, $(CD_3)_2SO$, 25 °C) δ = 27.3 (t, 1F, 11.1 Hz).

3,5-F_2Y−OMe·HCl: ^{1}H NMR (300 MHz, $(CD_3)_2SO$, 25 °C) δ = 3.05 (m, 2H, $C_\beta-H$), 3.70 (s, 3H, $-OCH_3$), 4.27 (m, 1H, $C_\alpha-H$), 6.94 (d, 2H, aromatic C−H, 8.8 Hz), 8.63 (b.s., 3H, $-NH_3^+$), 10.15 (s, 1H, PhO−H). ^{19}F NMR (300 MHz, $(CD_3)_2SO$, 25 °C) δ = 32.1 (d, 2F,11.1 Hz).

2,3-F_2Y−OMe·HCl: ^{1}H NMR (300 MHz, $(CD_3)_2SO$, 25 °C) δ = 3.09 (m, 2H, $C_\beta-H$), 3.65 (s, 3H, $-OCH_3$), 4.14 (m, 1H, $C_\alpha-H$), 6.78 (m, 1H, aromatic C−H), 6.89 (m, 1H, aromatic C−H), 8.64 (b.s., 3H, $-NH_3^+$), 10.51 (s, 1H, PhO−H). ^{19}F NMR (300 MHz, $(CD_3)_2SO$, 25 °C) δ = −0.5 (d, 1F, 22.2 Hz), 19.5 (d, 1F, 22.2 Hz).

2,3,5-F_3Y−OMe·HCl: ^{1}H NMR (300 MHz, $(CD_3)_2SO$, 25 °C) δ = 3.12 (m, 2H, $C_\beta-H$), 3.69 (s, 3H, $-OCH_3$), 4.22 (m, 1H, $C_\alpha-H$), 7.10 (m, 1H, aromatic C−H), 8.70 (b.s., 3H, $-NH_3^+$), 10.83 (b.s., 1H, PhO−H). ^{19}F NMR (300 MHz, $(CD_3)_2SO$, 25 °C) δ = 5.5 (d, 1F, 16.7 Hz), 15.8, (s, 1F), 24.5 (s, 1F).

2,3,6-F_3Y−OMe·HCl: ^{1}H NMR (300 MHz, $(CD_3)_2SO$, 25 °C) δ = 3.07 (m, 2H, $C_\beta-H$), 3.64 (s, 3H, $-OCH_3$), 4.07 (m, 1H, $C_\alpha-H$), 6.73 (m, 1H, aromatic C−H), 8.70 (b.s., 3H, $-NH_3^+$), 11.13 (s, 1H, PhO−H). ^{19}F NMR (300 MHz, $(CD_3)_2SO$, 25 °C) δ = −4.8 (s, 1F), 22.3 (d, 1F, 22.2 Hz), 40.9 (m, 1F).

2,3,5,6-F_4Y−OMe·HCl: ^{1}H NMR (300 MHz, $(CD_3)_2SO$, 25 °C) δ = 3.16 (m, 2H, $C_\beta-H$), 3.66 (s, 3H, $-OCH_3$), 4.14 (m, 1H, $C_\alpha-H$), 8.75 (b.s., 3H, $-NH_3^+$), 11.56 (b.s., 1H, PhO−H). ^{19}F NMR (300 MHz, $(CD_3)_2SO$, 25 °C) δ = −0.6 (d, 2F, 16.7 Hz), 16.2, (d, 1F, 22.2 Hz), 40.9 (m, 1F).

Synthesis of *N*-Acetyl−F_n-tyrosinamide (Ac−F_nY-NH_2). In a typical synthesis, 460 μmol of F_nY-OMe in 5.2 mL of MeCN were stirred with 4 equiv of triethylamine and 3 equiv of acetic anhydride. The reaction was monitored by TLC (20:1 $CHCl_3$/MeOH). After 2 h, the solvent was removed in vacuo. The product was redissolved in MeOH followed by the removal of MeOH in vacuo (2×). The *N*-acetylated, methyl ester derivative was converted to the amide by stirring the compound at a concentration of 100 mM in $NH_{3(g)}$-saturated MeOH. The reaction was complete after 3 days. The solvent was removed in vacuo, and the product was purified by silica gel chromatography with 15:1 CH_2Cl_2/MeOH as the eluant. The product was characterized by ^{1}H and ^{19}F NMR as well as LR-ESI-MS. Yields of 80−95% were obtained for all analogues.

Ac−3-FY−NH_2: ^{1}H NMR (300 MHz, CD_3OD) δ = (s, 3H, Ac), (dd, 1H, $C_\beta-H_1$, 8.8 Hz, 14.0 Hz), (dd, 1H, $C_\beta-H_2$, 5.8 Hz, 14.0 Hz), (dd, 1H, $C_\alpha-H$, 5.8 Hz, 8.8 Hz), (m, 1H, aromatic C−H). ^{19}F NMR (300 MHz, CD_3OD) δ = (dd, 1F, 8.3 Hz, 19.4 Hz), (dd, 1F, 8.3 Hz, 19.4 Hz). LR-ESI-MS: *m*/*z* (−H) calcd 239.0, found 238.9.

Ac−3,5-F_2Y−NH_2: ^{1}H NMR (300 MHz, CD_3OD) δ = 1.92 (s, 3H, Ac), 2.75 (dd, 1H, $C_\beta-H_1$, 9.2 Hz, 13.9 Hz), 3.03 (dd, 1H, $C_\beta-H_2$, 5.5 Hz, 13.9 Hz), 4.55 (dd, 1H, $C_\alpha-H$, 5.7 Hz, 9.2 Hz), 6.83 (m, 2H, aromatic C−H). ^{19}F NMR (300 MHz, CD_3OD) δ = 25.2 (d, 2F, 8.3 Hz). LR-ESI-MS: *m*/*z* (−H) calcd 257.0, found 256.9.

Ac−2,3-F_2Y−NH_2: ^{1}H NMR (300 MHz, CD_3OD) δ = 1.90 (s, 3H, Ac), 2.85 (dd, 1H, $C_\beta-H_1$, 8.8 Hz, 14.0 Hz), 3.12 (dd, 1H, $C_\beta-H_2$, 5.8 Hz, 14.0 Hz), 4.61 (dd, 1H, $C_\alpha-H$, 5.8 Hz, 8.8 Hz), 6.83 (m, 1H, aromatic C−H). ^{19}F NMR (300 MHz, CD_3OD) δ = −3.12 (dd, 1F, 8.3 Hz, 19.4 Hz), 17.3 (dd, 1F, 8.3 Hz, 19.4 Hz). LR-ESI-MS: *m*/*z* (−H) calcd 257.0, found 256.9.

Ac−2,3,5-F_3Y−NH_2: ^{1}H NMR (300 MHz, CD_3OD) δ = 1.93 (s, 3H, Ac), 2.78 (dd, 1H, $C_\beta-H_1$, 8.4 Hz, 14.1 Hz), 3.03 (dd, 1H, $C_\beta-H_2$, 6 Hz, 14.3 Hz), 4.53 (dd, 1H, $C_\alpha-H$, 5.7 Hz, 8.2 Hz), 6.56 (m, 1H, aromatic C−H). ^{19}F NMR (300 MHz, CD_3OD) δ = −0.95 (t, 1F, 19.4 Hz), 10.48 (m, 1F), 19.05 (dd, 1F, 11.1 Hz, 27.7 Hz). LR-ESI-MS: *m*/*z* (−H) calcd 275, found 274.9.

Ac−2,3,6-F_3Y−NH_2: ^{1}H −NMR (300 MHz, CD_3OD) δ = 1.94 (s, 3H, Ac), 2.93 (dd, 1H, $C_\beta-H_1$, 8.8 Hz, 14 Hz), 3.17 (dd, 1H, $C_\beta-H_2$, 5.5 Hz, 13.8 Hz), 4.65 (dd, 1H, $C_\alpha-H$, 5.7 Hz, 13.8 Hz), 6.51 (m, 1H, aromatic C−H). ^{19}F NMR (300 MHz, CD_3OD) δ = −10.4 (m, 1F) 17.4 (d, 1F, 21 Hz) 36.2 (t, 1F, 12 Hz). LR-ESI-MS: *m*/*z* (−H) calcd 275, found 274.9.

Ac−2,3,5,6-F_4Y−NH_2: ^{1}H NMR (300 MHz, CD_3OD) δ = 1.92 (s, 3H, Ac), 2.96 (dd, 1H, $C_\beta-H_1$, 8.4 Hz, 14.4 Hz), 3.2 (dd, 1H, $C_\beta-H_2$, 6 Hz, 14.4 Hz), 4.64 (dd, 1H, $C_\alpha-H$, 6 Hz, 8.4 Hz). LR-ESI-MS: calcd 293, found 293.^{19}F NMR (300 MHz, CD_3OD) δ = −5.0 (dd, 2F, 6 Hz, 22.5 Hz), 12.6 (dd, 2F, 6 Hz, 22.5 Hz). LR-ESI-MS: *m*/*z* (−H) calcd 293, found 292.9.

4-Benzoyl-L-phenylalanyl-F_nY Methyl Ester Trifluoroacetic Acid (BPA−$F_nY-OMe\cdot CF_3COOH$). F_nY-OMe (0.432 mmol, 1.0 equiv), Boc-BPA−OH (160 mg, 0.432 mmol, 1.0 equiv), 1-(3-(dimethylamino)propyl)-3-ethylcarbodiimide hydrochloride (91 mg, 0.475 mmol, 1.1 equiv), and 1-hydroxybenzotriazole (HOBt) (64 mg, 0.475 mg, 1.1 equiv) were combined in a 50-mL round-bottom flask with 20 mL of methylene chloride. *N*-methylmorpholine (NMM) (175 μL, 1.73 mmol, 4 equiv) was added, and the solution was stirred overnight at room temperature. The solution was diluted to 75 mL with methylene chloride and washed with 2× 30 mL of 10% citric acid solution. The organic layer was dried over $MgSO_4$, and the solvent was removed in vacuo. The resulting clear oil was dissolved in a few mLs of methylene chloride

and loaded onto a 1-mm thick silica gel Chromatotron plate. The product was eluted with 3% methanol/methylene chloride and the solvent was removed in vacuo. The resulting clear oil was dissolved in 1:1 TFA/CH_2Cl_2 and stirred for 20 min at room temperature. The solvents were then evaporated under a stream of $N_{2(g)}$, and the resulting clear oil was dried under high vacuum. Trituration with CH_2Cl_2, followed by the dropwise addition of ether, resulted in the formation of white crystals, which were cooled to −20 °C and isolated by filtration (45−65% yield).

BPA−Y−OMe·CF$_3$COOH: ^{1}H NMR (300 MHz, $(CD_3)_2CO$, 25 °C) δ = 2.88−3.18 (m, 2H, C_β−H), 3.37 (m, 2H, C_β−H), 3.68 (s, 3H, −OCH_3), 4.62 (m, 1H, C_α−H), 4.88 (m, 1H, C_α−H), 6.78 (m, 2H, phenol-H), 7.15 (m, 2H, phenol-H), 7.30 (d, 2H, $C_6H_4OC_6H_5$, 7.7 Hz), 7.55 (m, 2H, $C_6H_4OC_6H_5$), 7.67 (m, 3H, $C_6H_4OC_6H_5$), 7.76 (m, 2H, $C_6H_4OC_6H_5$).

BPA−3-FY−OMe·CF$_3$COOH: ^{1}H NMR (300 MHz, $(CD_3)_2CO$, 25 °C) δ = 2.90−3.20 (m, 2H, C_β−H), 3.32−3.48 (m, 2H, C_β−H), 3.69 (s, 3H, −OCH_3), 4.63 (m, 1H, C_α−H), 4.96 (m, 1H, C_α−H), 6.85−7.04 (m, 2H, phenol-H), 7.14 (m, 1H, phenol-H), 7.32 (m, 2H, $C_6H_4OC_6H_5$), 7.50−7.82 (m, 7H, $C_6H_4OC_6H_5$)^{19}F NMR (300 MHz, $(CD_3)_2CO$, 25 °C) δ = 27.17 (m, 1F), 89.76 (s, 3F).

BPA−3,5-F$_2$Y−OMe·CF$_3$COOH: ^{1}H NMR (300 MHz, $(CD_3)_2CO$, 25 °C) δ = 2.89−3.25 (m, 2H, C_β−H), 3.38 (m, 2H, C_β−H), 3.70 (s, 3H, −OCH_3), 4.65 (m, 1H, C_α−H), 4.95 (m, 1H, C_α−H), 7.03 (m, 2H, phenol-H), 7.33 (d, 2H, $C_6H_4OC_6H_5$, 8.3 Hz), 7.56 (m, 2H, $C_6H_4OC_6H_5$), 7.62−7.85 (m, 5H, $C_6H_4OC_6H_5$). 19F NMR (300 MHz, $(CD_3)_2CO$, 25 °C) δ = 26.6 (s, 2F), 85.6 (s, 3F).

BPA−2,3-F$_2$Y−OMe·CF$_3$COOH: ^{1}H NMR (300 MHz, $(CD_3)_2CO$, 25 °C) δ = 2.93−3.49 (m, 4H, C_β−H), 3.69 (s, 3H, −OCH_3), 4.68 (m, 1H, C_α−H), 4.95 (m, 1H, C_α−H), 6.80 (m, 1H, phenol-H), 7.01 (m, 1H, phenol-H), 7.39 (d, 2H, $C_6H_4OC_6H_5$, 7.7 Hz), 7.56 (m, 2H, $C_6H_4OC_6H_5$), 7.63−7.86 (m, 5H, $C_6H_4OC_6H_5$).^{19}F NMR (300 MHz, $(CD_3)_2CO$, 25 °C) δ = −1.7 (m, 1F), 18.3 (m, 1F), 85.6 (s, 3F).

BPA−2,3,5-F$_3$Y−OMe·CF$_3$COOH: ^{1}H NMR (300 MHz, $(CD_3)_2$-CO, 25 °C) δ = 2.93−3.51 (m, 4H, C_β−H), 3.70 (s, 3H, −OCH_3), 4.68 (m, 1H, C_α−H, 5.04 (m, 1H, C_α−H), 7.11 (m, 1H, phenol-H), 7.41 (d, 2H, $C_6H_4OC_6H_5$, 7.7 Hz), 7.55 (m, 2H, $C_6H_4OC_6H_5$), 7.62−7.85 (m, 5H, $C_6H_4OC_6H_5$).^{19}F NMR (300 MHz, $(CD_3)_2CO$, 25 °C) δ = 7.93 (d, 1F, 22.2 Hz), 18.56 (m, 1F), 26.1 (s, 1F), 89.9 (s, 3F).

BPA−2,3,6-F$_3$Y−OMe·CF$_3$COOH: ^{1}H NMR (300 MHz, $(CD_3)_2$-CO, 25 °C) δ = 3.00−3.26 (m, 2H, C_β−H), 3.44 (m, 2H, C_β−H), 3.67 (s, 3H, −OCH_3), 4.66 (m, 1H, C_α−H), 5.12 (m, 1H, C_α−H), 6.76 (m, 1H, phenol-H), 7.41−7.85 (m, 9H, $C_6H_4OC_6H_5$).^{19}F NMR (300 MHz, $(CD_3)_2CO$, 25 °C) δ = −1.86 (m, 1F), 25.2 (d, 1F, 22.2 Hz), 44.1 (m, 1F), 90.0 (s, 3F).

BPA−2,3,5,6-F$_4$Y−OMe·CF$_3$COOH: ^{1}H NMR (300 MHz, $(CD_3)_2CO$, 25 °C) δ = 3.10−3.52 (m, 4H, C_β−H), 3.68 (s, 3H, −OCH_3), 4.65 (m, 1H, C_α−H), 5.05 (m, 1H, C_α−H), 7.46−7.85 (m, 9H, $C_6H_4OC_6H_5$). ^{19}F NMR (300 MHz, $(CD_3)_2CO$, 25 °C) δ = −2.42 (d, 2F, 22.2 Hz), 14.6 (d, 2F, 22.2 Hz), 85.6 (s, 3F).

Physical Measurements. ^{1}H and ^{19}F NMR spectra were recorded on a Varian 300 MHz NMR at the MIT Department of Chemistry Instrumentation Facility (DCIF). Aqueous samples for ^{1}H NMR and ^{19}F NMR were carried out in D_2O with 3-(trimethylsilyl)-propionic acid-d_4 (TSP) as an internal standard and $CFCl_3$ as an external standard, respectively. Nonaqueous ^{1}H and ^{19}F NMR were externally referenced to tetramethylsilane and $CFCl_3$, respectively. Steady-state absorption spectra were recorded on an Agilent 8453 Diode Array spectrophotometer.

pK_a Determination of Ac−F$_n$Y−NH$_2$ Analogues using UV Spectroscopy and ^{19}F NMR Spectroscopy. The pH of solutions containing 10 mM potassium phosphate and 200 mM KCl were adjusted using either KOH or HCl spanning a range of 2−13 at 0.3−0.5 pH unit intervals. The Ac−F$_n$Y−NH$_2$ was diluted into each solution, and the pH was measured before and after acquisition of the UV spectrum. The absorption at $\lambda_{max}(Y^-)$, the wavelength of maximum absorption for the deprotonated phenolate form, was plotted vs pH and the data fit to:

$$\frac{A(\mathrm{pH}) - A(\mathrm{pH}=2)}{A\,(\mathrm{pH}=13) - A(\mathrm{pH}=2)} = f_{Y^-} = \frac{10^{(\mathrm{pH}-\mathrm{p}K_a)}}{1+10^{(\mathrm{pH}-\mathrm{p}K_a)}} \qquad (1)$$

where A is absorbance at λ_{max}(Ac−Y^-−NH$_2$) and f_{Y^-} represents the fraction of the amino acid in the phenolate form.

To determine the pK_a of 2,3-F$_2$Y by ^{19}F NMR, the samples were prepared in a similar fashion as described above for the pK_a determinations by UV spectroscopy. After preparation of the sample in an Eppendorf tube, the pH was measured again, and the sample was transferred to an NMR tube. Spectra were externally referenced to $CFCl_3$ and ^{19}F NMR recorded at different pH values. The change in the chemical shift of each fluorine nucleus was plotted against pH and fit to:

$$\frac{\delta(\mathrm{pH}) - \delta(\mathrm{pH}=5.3)}{\delta\,(\mathrm{pH}=9.4) - \delta(\mathrm{pH}=5.3)} = f_{Y^-} = \frac{10^{(\mathrm{pH}-\mathrm{p}K_a)}}{1+10^{(\mathrm{pH}-\mathrm{p}K_a)}} \qquad (2)$$

Differential Pulse Voltammetry (DPV). DPV was performed on the Ac−F$_n$Y−NH$_2$s using a CV-50W instrument from Bioanalytical Systems as previously described.[46] Briefly, measurements were performed in a three-electrode glass cell with a glassy carbon working electrode, a platinum wire counter-electrode, and a Ag/AgCl/3M NaCl reference electrode. The glassy carbon electrode was polished with a water/alumina slurry and sonicated for ∼1 min prior to each measurement. Typically, the solution contained 150−200 μM of Ac−F$_n$Y−NH$_2$ in 10 mM potassium phosphate with 200 mM KCl as the supporting electrolyte. The pH of each solution was adjusted with 1 M HCl or 1 M KOH prior to addition of the analyte and spanned a range of 1−13 at 0.3−0.5 pH unit intervals. After addition of the analyte to the solution and immediately before each measurement, the pH was measured with a pH meter, and the solution was degassed by Ar sparging for 2 min. Measurements were made with the ferricyanide/ferrocyanide couple as an internal standard (0.408 V[47] vs NHE, pH 7). DPV parameters were as follows: scan rate, 10 mV/s; sample width, 17 ms; pulse amplitude, 50 mV; pulse width, 50 ms; pulse period, 200 ms; quiet time, 4 s; sensitivity, 100 μA/V; temperature, 25 °C.

Generation of Oxidized F$_n$Ys and EPR Measurements. A 10−15 mM solution of each F$_n$Y was adjusted to pH 11 with NaOH. The sample was transferred to an EPR tube, and the solution bubbled with Ar for 15 min. The tube was then sealed under Ar pressure and quick-frozen in liquid N_2. The tube was immersed in liquid N_2 in a quartz finger dewar and irradiated for 5 min using unfiltered light from a 1000 W high pressure Xe arc lamp. The photolyzed product was never allowed to warm above 77 K, and the EPR spectra were subsequently recorded on a Bruker ESP-300 X-band (9.4 GHz) spectrometer equipped with an Oxford liquid He cryostat at 77 K. The EPR parameters were as follows: power = 0.2 mW; modulation frequency = 100 kHz; modulation amplitude = 1.5 G; time constant = 5.12 ms; and conversion time = 20.48 ms. The resulting EPR spectra remained unchanged after storage of the photolyzed product for one month at 77 K in the dark. The EPR spectra of 3-FY−R2 and wild-type (wt)-R2 (vide infra) were obtained at 25 K using the same parameters listed above, except with a modulation amplitude = 2 G. The 3-FY−R2 spectrum was simulated using SIMPIP and QPOW programs obtained from the Illinois EPR Research Center.

Transient Absorption (TA) Spectroscopy. Pump light for TA measurements was provided by an Infinity Nd:YAG laser (Coherent) running at 20 Hz. The setup of the instrument was slightly modified from that previously described.[48] The third harmonic (355 nm, 200 mJ per pulse) was used to pump a Type II XPO (Coherent). The 600-nm

(46) Tommos, C.; Skalicky, J. J.; Pilloud, D. L.; Wand, A. J.; Dutton, P. L. *Biochemistry* **1999**, *38*, 9495.
(47) O'Reilly, J. E. *Biochim. Biophys. Acta* **1973**, *292*, 509.

signal beam was isolated, and the frequency was doubled in a XPO-UV frequency-doubling crystal (Coherent) to produce a slightly divergent 300-nm beam with a ~5-ns pulse width and a pulse energy of ~500 μJ. This beam was then passed through a slow-focusing lens and through the sample at ~160°, producing a beam spot of 2-mm diameter on the sample. A 75 W Xe arc lamp (unpulsed, PTI) provided the probe light, which was focused onto the sample, overlapped with the pump beam, recollimated after the sample, and focused onto the entrance slit of a Triax 320 spectrometer. The probe beam was dispersed by a 300 × 500 blazed grating and collected with either an intensified gated CCD camera (ICCD, Andor Technology, 1024 pixels × 256 pixels, 26 μm^2) for TA spectra or a photomultiplier tube (PMT) for TA kinetics at a single wavelength. PMT outputs were collected and averaged with a 1 GHz oscilloscope (LeCroy 9384CM). To produce a TA spectrum, a series of four spectra were taken: I_F (pump on/probe off), I (pump on/probe on), I_B (pump off/probe off), and I_0 (pump off/probe on). Uniblitz shutters driven by delay generators (DG535, Stanford Research Systems) and T132 Uniblitz shutter drivers were used to block the pump and probe light in this sequence using a TTL trigger from the Q-switch of the laser. Transient spectra were corrected for fluorescence and background light using these spectra and the equation: $\Delta OD = \log[(I_0 - I_B)/(I - I_F)]$. Spectra reported are the average of 1250 of the four-spectra sequences. The instrument control and data analysis were performed by software written in LabView. Aqueous BPA−F_nY−OMe samples were prepared at 200−500 μM concentrations in deionized water buffered to pH 4 with 20 mM succinic acid. All TA measurements were performed in a 2-mm quartz optical cell. For BPA−3-FY−OMe, 266-nm pump light was used as described previously,[49] and the sample was flowed through a 2-mm cell to ensure fresh sample for each laser shot.

Computational Methods. Density functional theory calculations (DFT) were performed using the Amsterdam Density Functional (ADF2002.02) program,[50,51] a home-built Linux cluster comprising 60 Intel processors organized in groups of 12 running in parallel. The generalized gradient approximation was used as implemented in ADF by the Becke-88 functional for exchange[52] and the Perdew−Wang-91functional for correlation.[53] A basis set of triple-ζ Slater-type functions augmented by a polarization set (TZP) was used for all atoms; spin restriction was lifted for all Ac−F_nY•−NH_2 radicals. Energies reported are gas-phase internal energies at 0 K, without zero-point vibrational energy, of the geometry optimized structure. Each structure was optimized from the same amino acid backbone configuration, which was kept nearly constant throughout the calculation. Orbital energies, Cartesian coordinates, and atom-numbering schemes for each of the protonated, deprotonated, and radical Ac−F_nY−NH_2s are provided in the Supporting Information.

Global Incorporation of 3-FY into R2. Competent BL21(DE3) cells were transformed with pTB2, an R2 overexpression plasmid, and grown on an LB agar plate containing 100 mg/L ampicillin. A single colony from the plate was used to seed a 200-mL culture containing 100 mg/L ampicillin. The culture was grown overnight and then centrifuged at 10 000*g* for 10 min. The cell pellet was re-suspended in 50 mL of minimal medium containing no L-tyrosine and 100 mg/L ampicillin (details of the medium are reported in Supporting Information, Table S1). The doubling time of the cells was typically ~40 min, and at $A_{600\ nm}$ of 0.6, 1 g/L of 3-FY was added to the culture. IPTG (0.5 mM) was added to the culture 15 min after the addition of 3-FY. The cells were grown to $A_{600\ nm}$ of 1.4−1.6 and harvested ~4 h after induction. The yield was 5 g/L and 20−25 mg/g of cells, similar to yields obtained for wt R2 culture growths. 3-FY−R2 was purified using published procedures.[54]

Extent of Incorporation of 3-FY into R2. The purified 3-FY−R2 (200−2000 pmol) was lyophilized to dryness in a Speedvac and hydrolyzed in 200 μL of 6 N HCl (Pierce Sequence Grade) at 150 °C for 1 h or 110 °C for 22 h under N_2, with norleucine (1000 pmol) added as an internal standard. The samples were then dried in vacuo, treated with 2% borane/diisopropyl ethylamide complex solution (40 μL) to reduce methionine oxidation, and allowed to air-dry for 2 h. The samples were then dissolved in 0.3 M sodium acetate buffer (pH 5.5) containing 0.025% w/v potassium EDTA, mixed rigorously, and centrifuged at 15 000*g* on a tabletop centrifuge for 5 min to remove particulate matter. Aliquots (30 μL) were then loaded onto an Applied Biosystem model 420A Derivatizer using phenyl isothiocyanate as the derivatizing agent, followed by automatic injection onto an Applied Biosystem 130A Separation System, which uses a Spheri-5 PTC 5 micron, 220 mm × 2.1 mm column from Perkin-Elmer Brownlee. A series of pure amino acid standards, including 3-FY (500 pmol), were also derivatized and analyzed to determine the retention time of each amino acid and for quantitation purposes. The data were collected and analyzed using a Perkin-Elmer Applied Biosystem 610A Data Analysis program by the MIT Biopolymers Lab.

Results and Discussion

pK_a Determination of Ac−F_nY−NH_2s by UV Spectroscopy and 2,3-F_2Y by ^{19}F NMR. A slightly modified method from that of Kim and Cole[43] and Phillips and co-workers,[55] using TPL-mediated enzymatic synthesis, yields the free F_nYs in good yields and high purity. The amine and acid functionalities of the free amino acids were protected by acetylation and amidation to avoid complications arising from different protonation states of these groups. Figure 1 presents the absorption spectra of phenol and phenolate forms of the Ac−F_nY−NH_2 amino acids presented in Chart 1. Substitution of the aromatic protons of tyrosine with fluorine results in a blue-shift of the λ_{max} associated with the $\pi \rightarrow \pi^*$ transition (top panel), which red-shifts upon deprotonation (bottom panel). This observed bathochromic shift with deprotonation of the phenol group allows for the measurement of pK_a by UV spectroscopy.

The typical absorbance changes for Ac−F_nY−NH_2s induced by changes in pH are shown in Figure 2 for Ac−2,3-F_2Y−NH_2. The pK_a values were determined by plotting f_{Y^-} as a function of pH and fitting the data to eq 1 (see inset). The pK_a values listed in Table 1 for the protected Ac−F_nY−NH_2 amino acids differ from those previously determined for the unprotected F_nY analogues.[43] *N*-acetyl and C-amide protected derivatives allow us to monitor acid/base equilibria resulting only from the fluorophenol moiety; therefore, the pK_a values obtained on these blocked derivatives better approximate the pK_a that these residues would have in a solvent-exposed, simple polypeptide chain. The pK_a values of F_nY may be independently determined by ^{19}F NMR. Figure 3 shows the pH dependence of the two fluorine signals of 2,3-F_2Y; as the pH is decreased, these signals shift downfield. When the chemical shift is plotted as a function of pH and fit to eq 2, pK_as of 7.53 (using the lower field ^{19}F nucleus) and 7.59 (using the higher field ^{19}F nucleus) are obtained, in good agreement with that previously reported for

(48) Loh, Z.-H.; Miller, S. E.; Chang, C. J.; Carpenter, S. D.; Nocera, D. G. *J. Phys. Chem. A* **2002**, *106*, 11700.
(49) Reece, S. Y.; Stubbe J.; Nocera, D. G. *Biochim. Biophys. Acta* **2005**, *1706*, 232.
(50) te Velde, G.; Bickelhaupt, F. M.; van Gisbergen, S. J. A.; Fonseca Guerra, C.; Baerends, E. J.; Snijders, J. G.; Ziegler, T. *J. Comput. Chem.* **2001**, *22*, 931.
(51) Fonseca Guerra, C.; Snijders, J. G.; te Velde, G.; Baerends, E. J. *Theor. Chem. Acc.* **1998**, *99*, 391.
(52) Becke, A. D. *Phys. Rev. A* **1988**, *38*, 3098.
(53) Perdew, J. P.; Chevary, J. A.; Vosko, S. H.; Jackson, K. A.; Pederson, M. R.; Singh, D. J.; Fiolhais, C. *Phys. Rev. B* **1992**, *46*, 6671.
(54) Ge, J.; Yu, G.; Ator, M. A.; Stubbe, J. *Biochemistry* **2003**, *42*, 10071.
(55) Phillips, R. S.; Ravichandran, K.; Von Tersch, R. L. *Enzyme Microb. Technol.* **1989**, *11*, 80.

Table 1. Physical Data for Tyrosine and Fluorotyrosine Derivatives

derivative	λ_{max}(Ac–F_nY–NH_2) / nm (ϵ/M^{-1} cm^{-1})	λ_{max}(Ac–F_nY^-–NH_2) / nm (ϵ/M^{-1} cm^{-1})	λ_{max}($F_nY\bullet$)[a] / nm	pK_a[b]	pK_a[c]	pK_a[d]	E_p($Y\bullet$/Y^-) / mV[e]	δ(O–H) / ppm[f]
Y	275 (1400)	293 (2420)	407	10	–	9.9	642	9.44
3-FY	272 (1530)	289 (2740)	400	8.4	8.4	8.4	705	9.88
3,5-F_2Y	263 (560)	275 (1830)	395	6.8	7.2	7.2	755	10.15
2,3-F_2Y	265 (910)	279 (2060)	408	7.6	7.7	7.8	810	10.51
2,3,5-F_3Y	267 (570)	276 (1460)	400	6.1	6.4	6.4	853	10.83
2,3,6-F_3Y	266 (1050)	277 (2360)	415	6.6	6.9	7.0	911	11.13
F_4Y	~257 (420)	~273 (1660)	411	5.2	5.6	5.6	968	11.56

[a] BPA–F_nY–OMe dipeptides. [b] F_nY pK_a as reported in ref 43. [c] Ac–F_nY–NH_2 pK_a as determined by the UV–vis absorption titration method. [d] Ac–F_nY–NH_2 pK_a as determined by the DPV method. [e] DPV peak potential vs NHE for the Ac–F_nY$\bullet$–NH_2/Ac–$F_n$$Y^-$ –NH_2 couple. [f] F_nY–OMe ^{1}H NMR in $(CD_3)_2SO$.

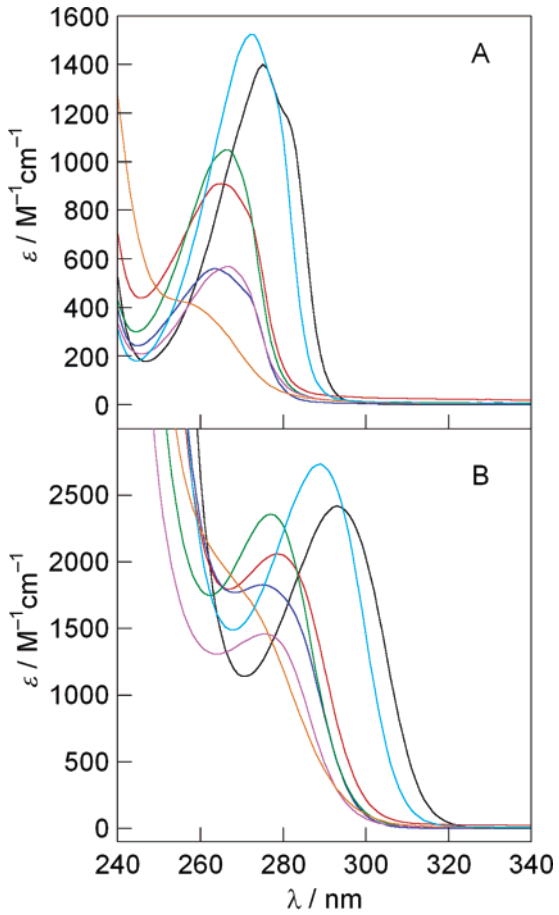

Figure 1. UV spectra of phenol (A) and phenolate (B) forms of (black —) Ac–Y–NH_2, (light blue —) Ac–3-FY–NH_2, (dark blue —) Ac–3,5-F_2Y–NH_2, (red —) Ac–2,3-F_2Y–NH_2, (green —) Ac–2,3,6-F_3Y–NH_2, (purple —) Ac–2,3,5-F_3Y–NH_2, and (orange —) Ac–F_4Y–NH_2.

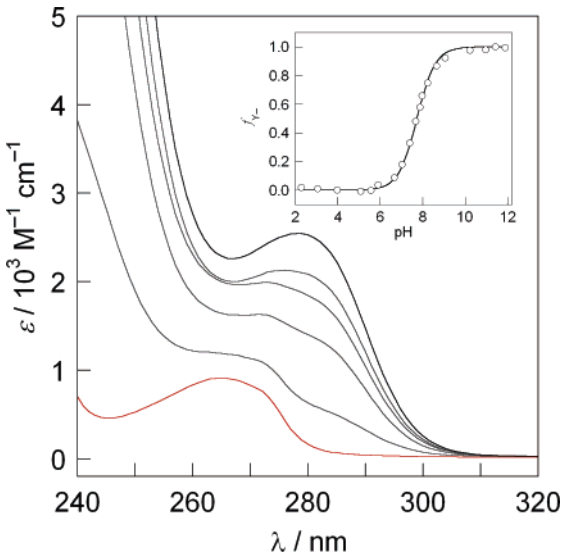

Figure 2. Changes in the absorption profile of Ac–2,3-F_2Y–NH_2 at aqueous solution pH of 5.1 (red —), 7.0, 7.7, 8.0, 8.3, and 9.1 (black —). (Inset) Fraction of Ac–2,3-$F_2$$Y^-$ –NH_2 vs pH (○) and fit (—) as described by eq 1.

the unprotected amino acid (pK_a = 7.6).[43] Within a protein environment, the determination of pK_a values of F_nYs by the ^{19}F NMR method may be easier to implement since large UV absorptions from intraprotein Y and W residues will obscure the bathochromic shift of F_nY residues incorporated into the protein. Indeed, ^{19}F NMR signals of nonnatural F_nY amino acids have been used in small proteins to probe changes in the environment of specific residues upon domain movements.[56]

pH-Dependent Oxidation of Ac–F_nY–NH_2's. Oxidation of Y is an irreversible one-electron event,[57] and thus, only peak potentials, E_p, may be obtained, most accurately by DPV.[46] Sample DPV traces for oxidation of each Ac–$F_n$$Y^-$–$NH_2$ are provided in Figure S2. Plots of E_p vs pH for the Ac–F_nY–NH_2 amino acids are shown in Figure 4. At pH values exceeding the pK_a of each Ac–F_nY–NH_2, a pH-independent peak potential is observed, indicative of the Ac–F_nY$\bullet$–NH_2/Ac–$F_n$$Y^-$ –NH_2 couple, and these values are listed in Table 1. As the pH is decreased below the pK_a, the peak potential increases by 59 mV per pH unit corresponding to the Ac–F_nY$\bullet$–NH_2/Ac–F_nY–NH_2 redox couple in which tyrosine oxidation is accompanied by proton loss. The pH dependence of E_p is in accordance with the Nernst equation,

$$E_p = E_p(\text{Ac–Y}\bullet\text{–NH}_2/\text{Ac–Y}^-\text{–NH}_2) + 2.3\,RT/nF\,\log\,(1 + 10^{-\text{pH}}/10^{-\text{p}K_a}) \quad (3)$$

where E_p(Ac–Y$\bullet$–NH_2/Ac–Y^- –NH_2) is the peak potential of the deprotonated tyrosinate and the pK_a accounts for the Ac–Y–NH_2 → Ac–Y^- –NH_2 + H^+ reaction. Square schemes describing the thermodynamics for oxidation[58] of tyrosine show that it is energetically disadvantageous to oxidize YH and then deprotonate (ET/PT) and likewise to deprotonate YH followed by oxidation (PT/ET).[36] Excepting extreme thermodynamic conditions,[36] the diagonal pathway of concerted electron–proton (CEP) is preferred for tyrosine oxidation.[59] It is likely operating

(56) Bonaccio, M.; Ghaderi, N.; Borchardt, D.; Dunn, M. F. *Biochemistry* **2005**, *44*, 7656.
(57) Harriman, A. *J. Phys. Chem.* **1987**, *91*, 6102.
(58) Mayer, J. M. *Annu. Rev. Phys. Chem.* **2004**, *55*, 363.
(59) Sjödin, M.; Styring, S.; Åkermark, B.; Sun, L.; Hammarström, L. *J. Am. Chem. Soc.* **2000**, *122*, 3932.

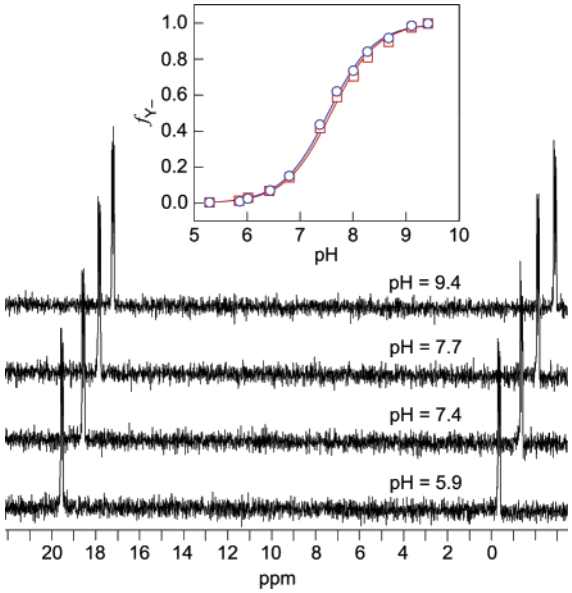

Figure 3. Dependence of ^{19}F NMR chemical shifts on pH. ^{19}F NMR spectra of free 2,3-F_2Y at various pH values (bottom) and fraction of 2,3-F_2Y^- as a function pH fit to eq 2 (top inset). Blue data points represent the signal of the higher -field ^{19}F nucleus; red data points represent that of the lower-field ^{19}F nucleus.

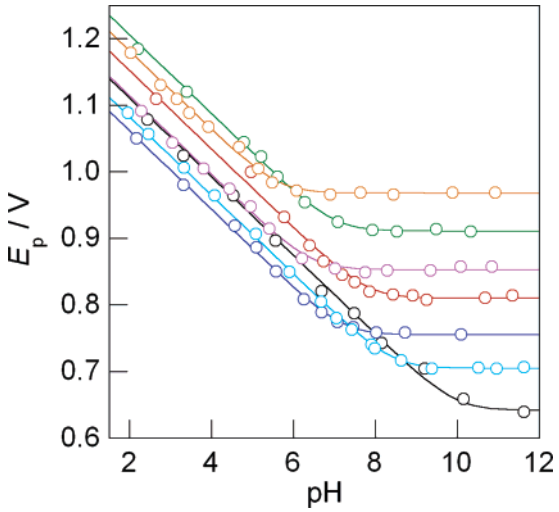

Figure 4. Reduction potential vs NHE as a function of pH for Ac−F_nY−NH_2 derivatives of Chart 1: (black —) Ac−Y−NH_2, (light blue —) Ac−3-FY−NH_2, (dark blue —) Ac−3,5-F_2Y−NH_2, (red —) Ac−2,3-F_2Y−NH_2, (purple —) Ac−2,3,5-F_3Y−NH_2, (green —) Ac−2,3,6-F_3Y−NH_2, and (orange —) Ac−F_4Y−NH_2.

here, too, for the flourotyrosines, though more detailed investigations are needed to establish unequivocally the mechanism of oxidation. A fit of the E_p vs pH curves in Figure 4 to eq 3 yields pK_as for Ac−F_nY−NH_2s that are in good agreement with those obtained using the UV titration method already described (see Table 1). The pK_a of the oxidized $[F_nY\bullet]^+$ radicals cannot be determined from eq 3 because water is oxidized at potentials below that needed for the electrochemical generation of $[F_nY\bullet]^+$ at low pHs.

Electronic-Structure Calculations of Ac−F_nY−NH_2s. The Ac−F_nY•−NH_2/Ac−F_nY^- −NH_2 redox couple was found to generally increase with the number of fluorine substituents on the phenol ring. Within the series of di- and trifluorotyrosines, the couples follow a trend: Ac−2,3-F_2Y−NH_2 > Ac−3,5-F_2Y−NH_2 and Ac−2,3,6-F_3Y−NH_2 > Ac−2,3,5-F_3Y−NH_2, which

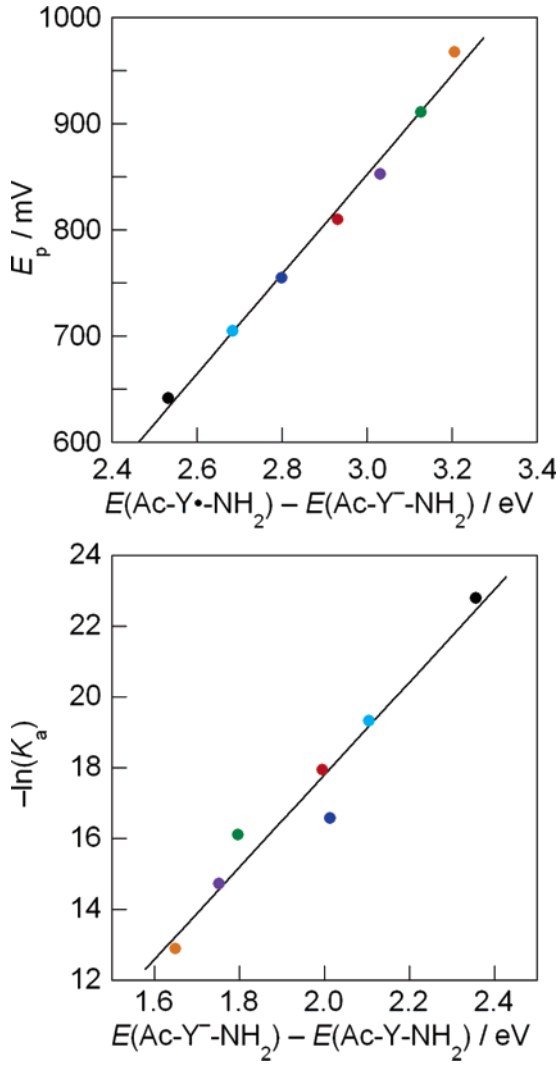

Figure 5. (Top) Plot of E_P(Ac−F_nY•−NH_2/Ac−F_nY^- −NH_2) vs E(Ac−F_nY•−NH_2) − E(Ac−F_nY^- −NH_2), the total bonding energy difference between Ac−F_nY•−NH_2 and Ac−F_nY^- −NH_2 as calculated by DFT, with linear fit (—). (Bottom) Plot of −ln(K_a) vs E(Ac−F_nY^- −NH_2) − E(Ac−F_nY−NH_2), the total bonding energy difference between Ac−F_nY^- −NH_2 and Ac−F_nY−NH_2 as calculated by DFT, with linear fit (—). Color coded points correspond to data for (black ●) Ac−Y−NH_2, (light blue ●) Ac−3-FY−NH_2, (dark blue ●) Ac−3,5-F_2Y−NH_2, (red ●) Ac−2,3-F_2Y−NH_2, (purple ●) Ac−2,3,5-F_3Y−NH_2, (green ●) Ac−2,3,6-F_3Y−NH_2, and (orange ●) Ac−F_4Y−NH_2.

is captured computationally. Geometry optimizations on Ac−F_nY−NH_2, Ac−F_nY•−NH_2, and Ac−F_nY^- −NH_2 were performed while keeping the amino acid backbone in the same conformation. Figure 5 (top) compares the difference in total bonding energy between the Ac−F_nY•−NH_2 and Ac−F_nY^- −NH_2 redox states, as calculated by DFT to the experimentally determined E_ps (Ac−F_nY•−NH_2/Ac−F_nY^- −NH_2). The linear correlation between observed and calculated results validates the quality of the computation. The electronic-structure calculation summarized in Figure 6 shows that the observed trend in the reduction potential arises primarily from stabilization of the HOMO and HOMO−1 orbitals of the phenolate with increasing fluorination of the aromatic ring of tyrosine. This stabilization of HOMO and HOMO−1 levels is most pronounced for Ac−F_nY^- −NH_2; these levels exhibit only a modest shift for Ac−F_nY•−NH_2 (and Ac−F_nY−NH_2) (see Figures S3−S5). The Kohn−Sham representations of the frontier molecular orbitals,

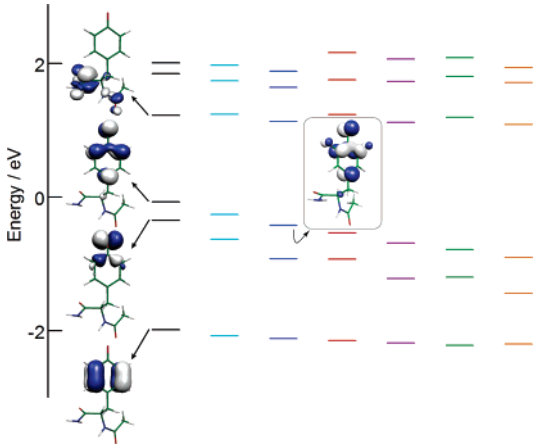

Figure 6. Energy-level diagram for frontier molecular orbitals of the phenolates: (black —) Ac−Y^- −NH_2, (light blue —) Ac−3-FY^- −NH_2, (dark blue —) Ac−3,5-F_2Y^- −NH_2, (red —) Ac−2,3-F_2Y^- −NH_2, (purple —) Ac−2,3,5-F_3Y^- −NH_2, (green —) Ac−2,3,6-F_3Y^- −NH_2, and (orange —) Ac−F_4Y^- −NH_2. Selected Kohn−Sham representations of orbitals for the tyrosine analogue are shown at the 95% probability level. Kohn−Sham representation of the HOMO orbital for Ac−3,5-F_2Y^- −NH_2 is presented in the frame.

shown for tyrosinate in Figure 6, reveal that the HOMO orbital carries significant π-electron density at the 3 and 5 positions of the aromatic ring, whereas the HOMO−1 has π-electron density localized on the orbital of the oxygen of the phenol, in an in-plane antibonding interaction with the aromatic ring. The interaction of the HOMO and HOMO−1 ring orbitals with the pπ-orbitals of the fluorine atom substituents allows subtle variations in the reduction potential among members of the phenolate series to be understood. For instance, substitution of fluorine at the 2,3 vs 3,5 ring positions results in a 65 mV increase in the reduction potential of the radical. The HOMO of Ac−3,5-F_2Y^-−NH_2, which is presented in the framed box of Figure 6, exhibits an antibonding interaction between the π-orbitals of the fluorine atoms and the 3,5-carbon pπ-orbitals of the aromatic ring. By moving a fluorine from a 5 to a 2 position, this antibonding interaction is relaxed significantly, resulting in stabilization of the HOMO. A similar effect is observed for 2,3,5- and 2,3,6-trifluorotyrosines.

A parallel calculation was performed to assess the difference between the observed ln(K_a) and the total bonding energy difference of protonated and deprotonated Ac−F_nY−NH_2s. The calculation predicts the general trend that increasing the number of fluorine substituents decreases the pK_a of the phenolic proton (Figure 5, bottom), however a poorer correlation is observed as compared to that for the reduction potentials. The anomaly is most obvious for Ac−2,3-F_2Y−NH_2 and Ac−3,5-F_2Y−NH_2, which are calculated to have similar pK_as despite an observed difference of 0.6 pK_a units. We believe that such deviations arise from the deficiency of gas-phase DFT calculations in modeling specific hydrogen-bonding interactions that are important in determining the overall pK_a of the fluorotyrosines.[60−62]

Spectroscopic Characterization of F_nY•. Distinct EPR signals are observed for oxidized Y and F_nYs. The oxidized species were generated by the method of Hulsebosch et al.,[63] using UV photolysis at 77 K. The spectra obtained are shown

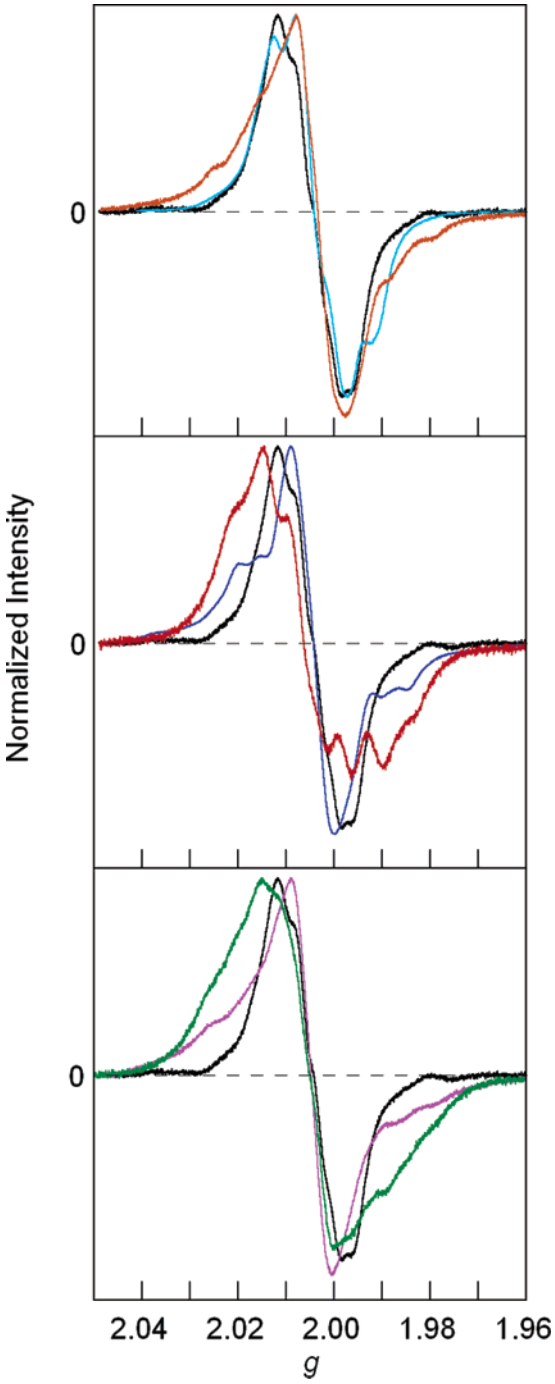

Figure 7. Normalized EPR spectra of oxidized: (black —) Y, (light blue —) 3-FY, (dark blue —) 3,5-F_2Y, (red —) 2,3-F_2Y, (purple —) 2,3,5-F_3Y, (green —) 2,3,6-F_3Y, and (orange —) F_4Y at 77 K. Oxidized product was formed by UV photolysis of pH 11 solutions of the F_nYs at 77K.

in Figure 7; the signal was stable for at least 1 month at 77 K. All F_nY•s display broader signals than Y•; lower modulation amplitudes and larger sweep widths did not uncover any additional hyperfine interactions. Qualitatively, the spectra of 2,3,5-F_3Y•, 2,3,6-F_3Y•, and 2,3,5,6-F_4Y• are similar, whereas those of 2,3-F_2Y• and 3,5-F_2Y• are distinctly different.

Attempts to simulate the EPR spectra displayed in Figure 7 by several methods were unsuccessful. Both standard programs

(60) Baker, A. W.; Kaeding, W. W. *J. Am. Chem. Soc.* **1959**, *81*, 5904.
(61) West, R.; Powell, D. L.; Whatley, L. S.; Lee, M. K. T.; Schleyer, P. von R. *J. Am. Chem. Soc.* **1962**, *84*, 3221.
(62) Carosati, E.; Sciabola, S.; Cruciani, G. *J. Med. Chem.* **2004**, *47*, 5114.
(63) Hulsebosch, R. J.; van den Brink, J. S.; Nieuwenhuis, S. A. M.; Gast, P.; Raap, J.; Lugtenburg, J.; Hoff, A. J. *J. Am. Chem. Soc.* **1997**, *119*, 8685.

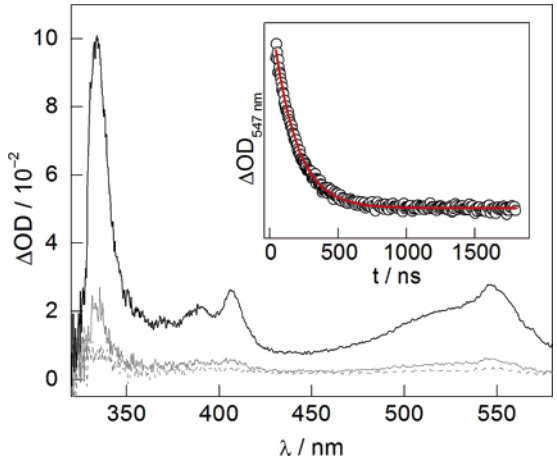

Figure 8. Transient absorption spectra recorded at (red —) 100 ns, (black —) 400 ns, and (green —) 1 μs following 300 nm, 5 ns excitation of a 500 μM solution of BPA−Y−OMe buffered to pH 4.0 with 20 mM succinic acid. Inset: Single wavelength kinetics of the 547 nm absorption (○) and the single-exponential decay fit (red —) to the data.

as well as DFT-based simulations were unsatisfactory, as has been previously observed with 3-FY• (David Britt, personal communication). These results suggest that frozen glasses of F_nY• contain a wide distribution of dihedral angles of the β-methylene hydrogen atoms. In Y•, one of these hydrogen atoms is responsible for the strongest hyperfine coupling to the unpaired electron.[63] Since the strength of this interaction varies as $\cos^2\theta$, where θ is the dihedral angle between the plane of the aromatic ring and the β-methylene hydrogen, a distribution over these angles can broaden the spectra.[64]

The absorption spectra of the fluorotyrosyl radical analogues in a dipeptide (BPA−F_nY−OMe) were obtained using the flash photolysis technique with benzophenone as the photooxidant of tyrosine. The triplet excited state of benzophenone has been shown to be a competent, bimolecular oxidant of tyrosine with an excited-state reduction potential of 1.69 V vs NHE and a bimolecular rate constant for the reaction with Y of $2.6 \pm 0.2 \times 10^9$ M^{-1} s^{-1}.[65] Moreover, the absorption spectrum of the benzophenone ketyl radical, produced upon tyrosine photooxidation, does not significantly overlap with that of the fluorotyrosyl radical analogue.

The photosensitized oxidation of tyrosine by benzophenone was accomplished by intramolecular ET within the dipeptide pair. Excitation of a solution of BPA−Y−OMe at pH 4.0 with a 300-nm nanosecond laser pulse produces a species with the transient absorption spectrum shown in Figure 8 at 100 ns. The strong, sharp peak with $\lambda_{max} = 334$ nm and broad peak at $\lambda_{max} = 547$ nm with a shoulder to the blue are the spectral signatures of the reduced benzophenone ketyl radical[66] ($\epsilon_{550\ nm}$(BPK•) = 3300 ± 700 M^{-1} cm^{-1} in cyclohexane),[67] whereas the absorption bands at $\lambda_{max} = 390$ and 407 nm are characteristic of Y• ($\epsilon_{410\ nm}$(Y•) = 2750 ± 200 M^{-1} cm^{-1}).[68] The Y• peak is slightly blue-shifted from that of free Y•, owing to their overlap with the tailing absorption of the 334 nm band of the ketyl radical of BPA (BPA•). The subsequent gray traces recorded at 400 ns and 1 μs show that the overall profile shape does not change with time. The transient signals decayed concomitantly with a rate constant of 5.6×10^6 s^{-1}; single wavelength kinetics data recorded at 547 nm are shown in the inset of Figure 8. This unimolecular decay is consistent with charge recombination between BPA• and Y•. The kinetics were unaffected by the presence or absence of oxygen in solution. A minor residual absorbance (<10%), which persists for tens of microseconds, is likely due to a small fraction of ET product formed in the bimolecular reaction between ^{3}BPA−Y−OMe and ground-state BPA−Y−OMe. This reaction is favored at the high concentrations of dipeptide required for the TA experiment.

Figure 9 shows the TA spectra obtained 100 ns after 300 nm excitation of each of the BPA−F_nY−OMe dipeptides. The amount of BPA•−F_nY•−OMe produced in each experiment varies due to changes in pump−probe beam overlap and sample concentration. Therefore, to allow for comparison of the F_nY• absorption maxima between experiments, the spectra in Figure 9 are normalized to the 547-nm peak of the BPA• ketyl radical. The feature is invariant for each of the dipeptides, whereas the absorption band of each F_nY• species varies in its maximum between 395 and 415 nm. The values of λ_{max} for each of the F_nY•s are listed in Table 1. An interesting comparison can be made between the F_nY•s and Y• absorbance features. The 2,3-F_2Y•, 2,3,6-F_3Y•, and F_4Y• all have the familiar double-hump absorbance feature of Y•, though they are slightly broader and red-shifted. The spectrum of 3-FY• also contains the double-hump feature, though its λ_{max} is now shifted to the blue by 7 nm. Of particular note are the single peaks at 395 and 400 nm for 3,5-F_2Y• and 2,3,5-F_3Y•, respectively, which are significantly blue-shifted from the larger 407 nm absorbance peak of Y•.

Incorporation of 3-FY into R2. To demonstrate the ability of F_nYs as spectroscopic probes of Y sites in biological systems, we replaced all Ys in R2 with 3-FY using global incorporation methods. The successful procedure required the growth of the bacteria in minimal media from which Y was omitted and replaced by 3-FY. Under these conditions, the doubling time of the bacteria was 40 min. SDS-PAGE analysis of whole cells after induction with IPTG suggests that the expression level of 3-FY−R2 is quite similar to that observed for wt R2 (20−25 mg/g of cell paste), which has a monomeric MW of ~43 kDa (Figure 10, lane 1). 3-FY−R2 was isolated using the standard isolation procedure for wt R2. SDS-PAGE analysis of purified 3-FY−R2 (Figure 10, lane 4) shows that the purified protein is ~90% homogeneous. Amino acid analysis indicates ~90% incorporation of 3-FY. EPR analysis of this material using wt *E. coli* R2 as an integration standard[69] revealed 0.6−0.8 FY•s/dimer. The absorption spectrum of the 3-FY122• (Figure S1, Supporting Information) shows that λ_{max} blue-shifts to 402 nm (wt Y122• has a λ_{max} of 411 nm), similar to the results from the TA experiments described above, suggesting that the protein environment is not perturbing the spectrum.

The EPR spectrum of wt R2 from *E. coli* has previously been characterized at 9, 35, 140, 195, 245, and 280 GHz and has anisotropic g values of $g_x = 2.00912-2.00868$, $g_y = 2.00457-2.0043$, and $g_z = 2.00225-2.00208$.[28] The X-band EPR spectrum of wt R2 is dominated by the well-resolved, nearly isotropic coupling to one of its β-Hs ($A_x = 61.2$ MHz, $A_y = A_z$

(64) Warncke, K.; Babcock, G. T.; McCracken, J. *J. Phys. Chem.* **1996**, *100*, 4654.
(65) Canonica, S.; Hellrung, B.; Wirz, J. *J. Phys. Chem. A* **2000**, *104*, 1226.
(66) Kajii, Y.; Itabashi, H.; Shibuya, K.; Obi, K. *J. Phys. Chem.* **1992**, *96*, 7244.
(67) Johnston, J. L.; Lougnot, D. J.; Wintgens, V.; Scaiano, J. C. *J. Am. Chem. Soc.* **1988**, *110*, 518.
(68) Feitelson, J.; Hayon, E. *J. Phys. Chem.* **1973**, *77*, 10.

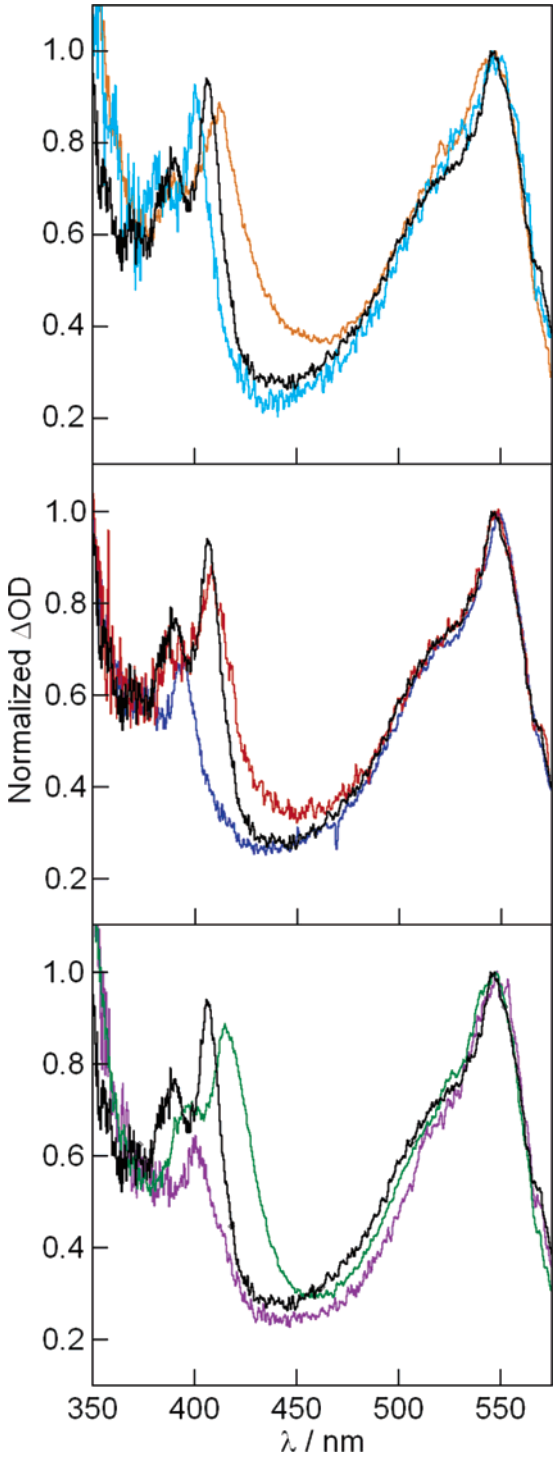

Figure 9. The transient absorption spectrum of (black —) BPA−Y−OMe, (light blue —) BPA−3-FY−OMe, (dark blue —) BPA−3,5-F_2Y−OMe, (red —) BPA−2,3-F_2Y−OMe, (purple —) BPA−2,3,5-F_3Y−OMe, (green —) BPA−2,3,6-F_3Y−OMe, and (orange —) BPA−F_4Y−OMe normalized to the peak at 547 nm obtained 100 ns after excitation of ∼500 μM solutions of each dipeptide buffered to pH 4.0 with 20 mM succinic acid.

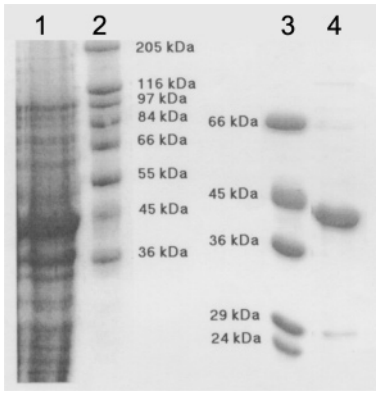

Figure 10. SDS gel analysis of 3-FY−R2 with lanes: (1) overexpression of 3-FY−R2, (2) high-range molecular weight marker, (3) low-range molecular weight marker, and (4) purified 3-FY−R2.

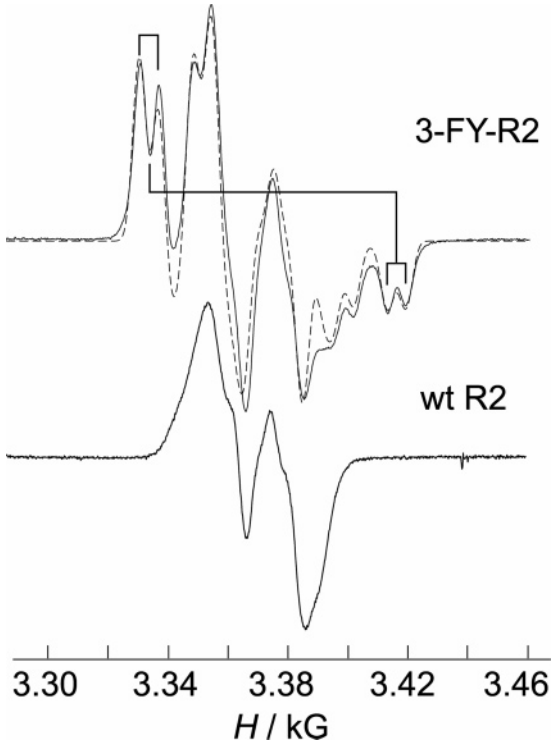

Figure 11. (Top) EPR spectrum (solid line) and simulation (dotted line) of 3-FY−R2 at 25 K. The values used for the simulation are listed in Table 2. (Bottom) EPR spectrum of wt R2 under the same conditions.

Table 2. *A*-Tensors of Nuclei with Significant Hyperfine Couplings in 3-FY•−R2

nucleus	A_x (MHz)	A_y (MHz)	A_z (MHz)	ϕ^a
P3-F	−15 (6)	−3 (4)	180 (2)	0
Pβ-H_1	48 (6)	54 (4)	50 (2)	0
P5-H	−25 (1)	−8 (1)	−17 (1)	25
P2,6-H	3	9	6	65

[a] ϕ angles describe rotation about the axis normal to the plane of the phenol ring between the **g** tensor and hyperfine tensors.

= 53.7 MHz).[70] The second β-H coupling is much smaller and is usually buried in the EPR line width.[71] This study presents the first observation of the magnetic properties of a 3-FY• in a protein. The X-band EPR spectrum of this radical, along with the simulation, is shown in Figure 11. Table 2 presents the *A*-tensors of the nuclei with significant hyperfine couplings to the unpaired electron. The splitting due to coupling to the β-H is similar to that observed for the Y122• in wt R2. However, a strongly split doublet of doublets, demarcated by brackets in Figure 11, is apparent at the extremes of the spectrum due to coupling to the fluorine nucleus. Together, the results above show that 3-FY can be incorporated at high efficiency into R2, yielding 3-FY−R2 with high radical content and activity. Further, the EPR spectrum shows that the 3-FY122• has well-

resolved hyperfine interactions that can be simulated, supporting our contention that the $F_nY\bullet$ EPR spectra of Figure 7 are broad due to a distribution in the dihedral angles of β-methylene hydrogens.

RNR activity is preserved with global substitution of the 14 Y residues of R2. The activity of the 3-FY−R2/R1 complex was measured by a coupled spectrophotometric assay using TR/TRR/NADPH as the source of reductant.[69] The specific activity obtained is ∼65%, that of wt R2, suggesting that substitution of the 14 Y residues in R2 with 3-FY minimally perturbs the tertiary structure of 3-FY−R2.

Conclusions

The mechanistic complexity arising from the coupling of electron and proton transfers in charge-transport processes involving amino acid radicals requires the development of new tools and methods for their study. We show here that F_nYs will be useful in the study of biological charge-transport mechanisms involving tyrosine for the following reasons. (1) They provide a range of pK_as for the phenolic proton and E_ps for the Y•/Y couple, which allows for tuning of the $\Delta G°_{PT}$ and $\Delta G°_{ET}$ for the PCET reaction. UV−vis and DPV analysis illustrate that the Ac−F_nY−NH_2's offer a range of almost 5 units in pK_a and 320 mV in redox potential within the pH range of 6−9, where proteins can be studied. (2) The oxidized forms of $F_nY\bullet$s possess unique spectral signals allowing a distinction between Y• and $F_nY\bullet$ in the same system. The time-resolved absorption spectra of BPA−F_nY−OMe dipeptides show that the λ_{max} for $F_nY\bullet$ absorption can be shifted by ∼10 nm relative to Y•. (3) In addition to glutathione transferase[72,73] and other proteins,[74−79] 3-FY can be incorporated into RNR with relatively minimal structural perturbation, as demonstrated by the preserved activity of the R2 subunit of class I *E. coli* RNR, in which 14 Y residues were globally replaced by 3-FY.

The F_nYs will be useful for a variety of mechanistic studies in biology, in which tyrosine is integral to radical initiation and transport. We demonstrate one example of this utility in the companion paper in which Y_{356} of R2 is site-specifically replaced with the F_nYs presented in this study. A study of the pH-dependent activity of each of these new semisynthetic enzymes cast with the backdrop of the Ac−F_nY−NH_2's pK_a and Ac−$F_nY\bullet$−NH_2's reduction potential data, reported herein, allows for mechanistic details of the PCET reactivity at this site to be unveiled.

Acknowledgment. We thank Prof. Robert Phillips for the generous gift of the plasmid, pTZTPL, used for encoding the enzyme tyrosine phenol lyase (TPL), Dave Bray of the MIT DCIF for help with Figure 3, Julien Bachmann for assistance with DFT calculations, R. David Britt for discussions regarding fitting of the $F_nY\bullet$ EPR spectra, Stoyan K. Smoukov and Brian M. Hoffman for fitting the EPR spectrum of 3-FY122•, Hiep-Hoa T. Nguyen for preparation of 3-FY−R2, Cyril S. Yee for initial work with Ac−2,3-F_2Y−NH_2, John H. Robblee for helpful discussions, and the National Institutes of Health for support of this work GM47274 (D.G.N.) and GM29595 (J.S.).

Supporting Information Available: Details of the *E. coli* growth medium for 3-FY−R2 preparation; the UV−vis spectrum of 3-FY−R2; sample different pulse voltammograms of Ac−Y^- −NH_2 and Ac−F_nY^- −NH_2s; Cartesian coordinates and atom-numbering scheme used for DFT calculations; MO energy-level diagrams of the tyrosine and fluorotyrosine derivatives. This material is available free of charge via the Internet at http://pubs.acs.org.

JA055926R

(69) Ge, J.; Perlstein, D. L.; Nguyen, H.-H.; Bar, G.; Griffin, R. G.; Stubbe, J. *Proc. Natl. Acad. Sci. U.S.A.* **2001**, *98*, 10067.
(70) Bender, C. J.; Sahlin, M.; Babcock, G. T.; Barry, B. A.; Chandrashekar, T. K.; Salowe, S. P.; Stubbe, J.; Lindström, B.; Petersson, L.; Ehrenberg, A.; Sjöberg, B.-M. *J. Am. Chem. Soc.* **1989**, *111*, 8076.
(71) Bar, G.; Bennati, M.; Nguyen, H. H.; Ge, J.; Stubbe, J.; Griffin, R. G. *J. Am. Chem. Soc.* **2001**, *123*, 3569.
(72) Parsons, J. F.; Armstrong, R. N. *J. Am. Chem. Soc.* **1996**, *118*, 2295.
(73) Xiao, G.; Parsons, J. F.; Armstrong, R. N.; Gilliland, G. L. *J. Am. Chem. Soc.* **1997**, *119*, 9325.
(74) Hull, W. E.; Sykes, B. D. *Biochemistry* **1976**, *15*, 1535.
(75) Kimber, B. J.; Griffths, D. V.; Birdsall, B.; King, R. W.; Scudder, P.; Freeney, J.; Roberts, G. C. K.; Burgen, A. S. V. *Biochemistry* **1977**, *16*, 3492.
(76) Sixl, F.; King, R. W.; Bracken, M.; Feeney, J. *Biochem. J.* **1990**, *266*, 545.
(77) Eccleston, J. F.; Molloy, D. P.; Hinds, M. G.; King, R. W.; Feeney, J. *Eur. J. Biochem.* **1993**, *278*, 1041.
(78) Lui, S. M.; Cowan, J. A. *J. Am. Chem. Soc.* **1994**, *116*, 4483.
(79) Pal, P. P.; Bae, J. H.; Azim, M. K.; Hess, P.; Friedrich, R.; Huber, R.; Moroder, L.; Budisa, N. *Biochemistry* **2005**, *44*, 3663.